



The potential mechanisms of the dominant timescale of AMOC multidecadal variability in CMIP6/CMIP5 preindustrial simulations

Xiaofan Ma^{1,2} · Gang Huang^{2,3,4} · Xichen Li⁵ · Shouwei Li⁶

Received: 7 November 2021 / Accepted: 24 July 2022 / Published online: 9 August 2022
© The Author(s), under exclusive licence to Springer-Verlag GmbH Germany, part of Springer Nature 2022

Abstract

Observations, theoretical analyses, and climate models show that the dominant timescale of multidecadal variability of the Atlantic Meridional Overturning Circulation (AMOC) is related to westward temperature propagations in the subpolar North Atlantic, which is modulated by oceanic baroclinic Rossby waves or thermal Rossby waves. Here, we find major timescales of AMOC variability of 12–28 years and associated westward temperature propagations in the preindustrial simulations of 9 CMIP6/CMIP5 models. The comparison with observations shows that the models reasonably simulate ocean stratifications and baroclinic Rossby waves in the subpolar North Atlantic. The timescale of the oceanic baroclinic Rossby wave propagating on a static background across the basin overestimates the major timescale of AMOC variability. The dual effects of the mean flow on the AMOC timescale are then considered, involving the eastward advection and the additional westward propagation (i.e., thermal Rossby wave) induced by the northward mean potential vorticity gradient. We find that the AMOC major timescale is generally determined by the comprehensive effects of the baroclinic Rossby wave and the mean flow effects, in which the additional westward propagation plays a dominant role. Our results illustrate the importance of considering mean flow effects in the estimate of the dominant timescale of AMOC multidecadal variability.

Keywords Atlantic meridional overturning circulation · Multidecadal variability · Westward temperature propagation · Oceanic baroclinic Rossby wave · Thermal Rossby wave · Mean flow effects

1 Introduction

Suggested by both observations (Cunningham et al. 2007; McCarthy et al. 2012) and climate models (Liu 2012; Buckley and Marshall 2016), the Atlantic Meridional Overturning Circulation (AMOC) has a rich diversity of variability from interannual to centennial timescales, which acts as an important source of climate variability over the Atlantic and surrounding regions (Sutton and Hodson 2005; Knight et al. 2006; Zhang and Delworth 2006; Zhang and Zhang 2015; Zhang et al. 2019; Ma et al. 2020) and a potential pacemaker for decadal climate predictions (Griffies and Bryan 1997; Zhang and Zhang 2015; Zhang et al. 2019).

The major and common timescale of AMOC multidecadal variability over the subpolar North Atlantic is suggested to be around 20–30 years in numerous models (Frankcombe et al. 2010; Zhang and Wang 2013; Muir and Fedorov 2017; Wu and Liu 2020) as well as in multiple paleo-records (Sicre et al. 2008; Chylek et al. 2012). The ~20–30 year AMOC variability has been described as a thermal Rossby mode based on the thermal wind relation between the zonal

✉ Gang Huang
hg@mail.iap.ac.cn

¹ Collaborative Innovation Center on Forecast and Evaluation of Meteorological Disasters (CIC-FEMD)/Institute for Climate and Application Research (ICAR), Nanjing University of Information Science & Technology (NUIST), Nanjing 210044, China

² State Key Laboratory of Numerical Modeling for Atmospheric Sciences and Geophysical Fluid Dynamics, Institute of Atmospheric Physics, Chinese Academy of Sciences, Beijing 100029, China

³ Laboratory for Regional Oceanography and Numerical Modeling, Qingdao National Laboratory for Marine Science and Technology, Qingdao 266237, China

⁴ University of Chinese Academy of Sciences, Beijing 100049, China

⁵ International Center for Climate and Environment Sciences, Institute of Atmospheric Physics, Chinese Academy of Sciences, Beijing 10029, China

⁶ Department of Earth and Planetary Sciences, University of California Riverside, Riverside, CA 92521, USA

density gradient and the meridional overturning circulation, and has also been illustrated to be related to the westward propagation of temperature anomalies in the subpolar North Atlantic (Colin de Verdiere and Huck 1999; Te Raa and Dijkstra 2002; Dijkstra et al. 2006; Frankcombe et al. 2008, 2010). The evidence of the westward temperature spreading has been identified not only in climate models (Frankcombe et al. 2010; Buckley et al. 2012; Sévellec and Fedorov 2013, 2015) but also in observations such as sea surface temperature (Feng and Dijkstra 2014), ocean subsurface temperature (Frankcombe et al. 2008) and sea surface height records (Frankcombe and Dijkstra 2009; Vianna and Menezes 2013).

Identification of the potential mechanisms behind this ~20–30 year AMOC variability has been a key issue in recent studies. To explain the AMOC-related westward temperature propagation, the so-called thermal Rossby mode is usually adopted, which suggested that the large east–west temperature (density) gradients in the North Atlantic can induce large anomalous northward currents at the surface, therefore lead to a strong AMOC and vice versa (Te Raa and Dijkstra 2002; Dijkstra et al. 2006; Sévellec and Fedorov 2013, 2015; Ortega et al. 2015). Previous studies have attributed the AMOC-related westward spread of temperature anomalies to the westward propagation of baroclinic ocean Rossby waves across the subpolar North Atlantic (Frankcombe et al. 2008; Buckley et al. 2012). Specifically, the AMOC variations are generated by a basin-scale adjustment of oceanic density over the North Atlantic, in which the timescale of the density adjustment is mainly controlled by the basin-crossing Rossby waves (Kawase 1987; Johnson and Marshall 2002). Ocean stratification is an important driver of the baroclinic Rossby wave speed and, in turn, the major timescale of AMOC variability, which has been discussed in model studies (Yang et al. 2012; Cheng et al. 2016; MacMartin et al. 2016; Armstrong et al. 2017; Wu and Liu 2020). Other possible factors affecting the wave propagation and AMOC variability might be the effects of mean zonal flow, including the eastward mean advection and the additional westward propagation induced by the northward mean potential vorticity gradient as illustrated in the concept of the non-Doppler shift effect (Rossby 1939; Killworth et al. 1997; Liu 1999). Several studies demonstrated that the AMOC-related westward spreading temperatures are generated by the interaction between the mean flow effects and the baroclinic Rossby waves over the subpolar North Atlantic (Sévellec and Fedorov 2013, 2015; Ortega et al. 2015; Muir and Fedorov 2017).

A more challenging issue is estimating the dominant timescales of AMOC variability based on the wave theory. Recent works have shown a shortened period of AMOC multidecadal variability under global warming, which can be captured by the enhanced ocean stratification and the

consequent speedup of baroclinic Rossby waves (Cheng et al. 2016; Wu and Liu 2020; Ma et al. 2021). However, the mean flow effects on wave propagations and AMOC timescales are rarely taken into account in previous studies. Sévellec and Fedorov (2013) analyzed the sensitivity of AMOC-related temperature oscillating period to different magnitudes in the additional westward propagation and the eastward mean advection in an idealized two-layer ocean model. They revealed two regimes of period changes featuring eastward or westward propagation, which depend on whether the eastward mean advection is stronger than the westward tendency resulting from both the additional westward propagation and the baroclinic Rossby wave. Nevertheless, a synthetic estimate of the major timescale of AMOC variability under the consideration of the baroclinic Rossby waves as well as the mean flow effects needs to be conducted in coupled climate models with more complex dynamics.

The different phases of the Coupled Model Intercomparison Project (CMIP) enable us to testify the robustness or uncertainties of the AMOC variability and the relevant mechanisms with identical simulations conducted by consecutive generations of models. By conducting the multi-model intercomparison, previous studies have found the ~20–30 year AMOC variability (Zhang and Wang 2013; Muir and Fedorov 2017) as well as the relevant evidence of westward spreading temperature signals (Muir and Fedorov 2017) in CMIP5 models. However, the timescales of AMOC variability in the latest generation of CMIP6 models (Eyring et al. 2016), which are necessary for a deeper understanding of internal climate variability, still remain unclear. In this study, we examine the AMOC multidecadal variability in the preindustrial run of 9 CMIP6/CMIP5 models. We focus on interpreting and estimating the major timescales of AMOC variability in all the 9 models by a uniform method using the wave theory. We find that both the oceanic baroclinic Rossby wave and the mean flow effects play roles in the explanation and estimate of the major timescales of AMOC variability.

2 Data and methods

We use the preindustrial runs in 9 coupled climate models (Table 1) including 3 CMIP5 (Taylor et al. 2012) and 6 CMIP6 (Eyring et al. 2016) models. The AMOC in these models has significant variabilities on multidecadal timescales. For each model, we download a 500-year simulation and interpolate all variables needed to a $1^\circ \times 1^\circ$ regular grid. The least-square linear trend in all model data is removed before analyses to exclude any climate drift. The annual mean data are used for every model. We also use 3 gridded observation products of oceanic temperature and salinity on time spans over the longest availability, including one Argo-based dataset, IPRC Argo plus Aviso altimetry (Argo 2020),

Table 1 Models used in this study

Model name	Spatial resolution of the ocean component (latxlon, vertical levels)	Spatial resolution of the atmosphere component (latxlon, vertical levels)	CMIP generation
FGOALS-g2	360×196, 30	128×60, 26	CMIP5
FGOALS-g3	218×360, 30	90×180, 26	CMIP6
GFDL-CM4	1080×1440, 75	180×360, 33	CMIP6
GISS-E2-R	180×288, 32	90×144, 40	CMIP5
IPSL-CM5A-LR	90×180, 31	96×95, 39	CMIP5
MIROC6	256×360, 63	128×256, 81	CMIP6
MRI-ESM2-0	364×360, 61	160×320, 80	CMIP6
NorESM2-MM	384×360, 70	192×288, 32	CMIP6
SAM0-UNICON	384×320, 60	192×288, 30	CMIP6

and two world-ocean atlases, WOA18 (Locarnini et al. 2018; Zweng et al. 2018) and Levitus94 (Levitus et al. 1994; Levitus and Boyer 1994).

The meridional streamfunction (ψ) is calculated by the meridional velocity (v) as

$$\psi(y, z) = \int_{x_e}^{x_w} \int_{-z}^0 v(x, y, z) dz dx \quad (1)$$

where x , y , and z are zonal, meridional, and vertical coordinates. x_w and x_e are western and eastern boundaries of the Atlantic basin. The mean meridional streamfunction in the Atlantic in the preindustrial simulations of the 9 models are shown in Fig. 1. The mean AMOC strength at 26°N in most models corresponds reasonably with the observation of the RAPID array (~17.8 Sv; Moat et al. 2020). The variations of meridional streamfunction in the Atlantic are mostly large at ~45°N among these models, as shown by the standard deviation pattern of the annual mean meridional streamfunction (Fig. 2). Therefore, we choose the maximum streamfunction at 45°N below 500 m depth as the AMOC index to investigate the AMOC multidecadal variability in this study.

3 Results

3.1 The AMOC variability

We investigate the AMOC variability in the preindustrial runs of the 9 CMIP6/CMIP5 models. We conduct power spectrum analysis on the AMOC indices at 45°N in the 500-year simulations. As shown in Fig. 3, these models exhibit diverse AMOC variability with greatly different magnitudes from interannual to multidecadal timescales. Nevertheless, all these models have significant peaks on timescales longer than a decade ranging from 12 to 28 years, which is consistent with previous CMIP5 studies (Muir and Fedorov 2017).

Specifically, 6 out of 9 models have major AMOC timescales falling in the ~20–30 year window, meanwhile, another 3 models display major AMOC timescales between 10 and 20 years (GFDL-CM4, MIROC6, MRI-ESM2-0). We will show that all the 10–30 year AMOC variability is related to the westward propagation of temperature anomalies over the subpolar North Atlantic.

3.2 The westward temperature propagation in relation to the AMOC multidecadal variability

We next examine the westward spreading of temperature signals related to the ~10–30 year AMOC variability in these 9 models. Figure 4 is the Hovmöller diagram on the time-longitude plane displaying the zonal propagation of temperature anomalies. For each model, the temperature anomalies are averaged over the subpolar North Atlantic (45°N–60°N, 80°W–0°) in the upper ocean (above ~1100 m where the ocean stratification has large variations, see Fig. 6). The temperature anomalies in each model are processed by a band-pass filter around the significant band of the AMOC spectral peak as denoted on the top-right corner in each plot of Fig. 4. The usage of band-pass filters helps isolate the timescale of interest, which has been applied in previous studies (e.g., Muir and Fedorov 2017; Gastineau et al. 2018; Årthun et al. 2021). In most models, there are clear westward temperature propagations with alternative positive and negative signs across the entire subpolar North Atlantic basin, consistent with the results in other CMIP5 models (Muir and Fedorov 2017). The westward propagating temperature anomalies have common timescales with the AMOC variability in most models. This could be supported by the power spectrum of the temperature anomalies averaged over the subpolar North Atlantic in a narrower latitude band (Fig. 5), which has peaks in the similar frequency bands to that in the AMOC spectrum (Fig. 3) in most models. The model uncertainty exists that the westward propagations are mostly confined to central parts of the basin in the GISS-E2-R and

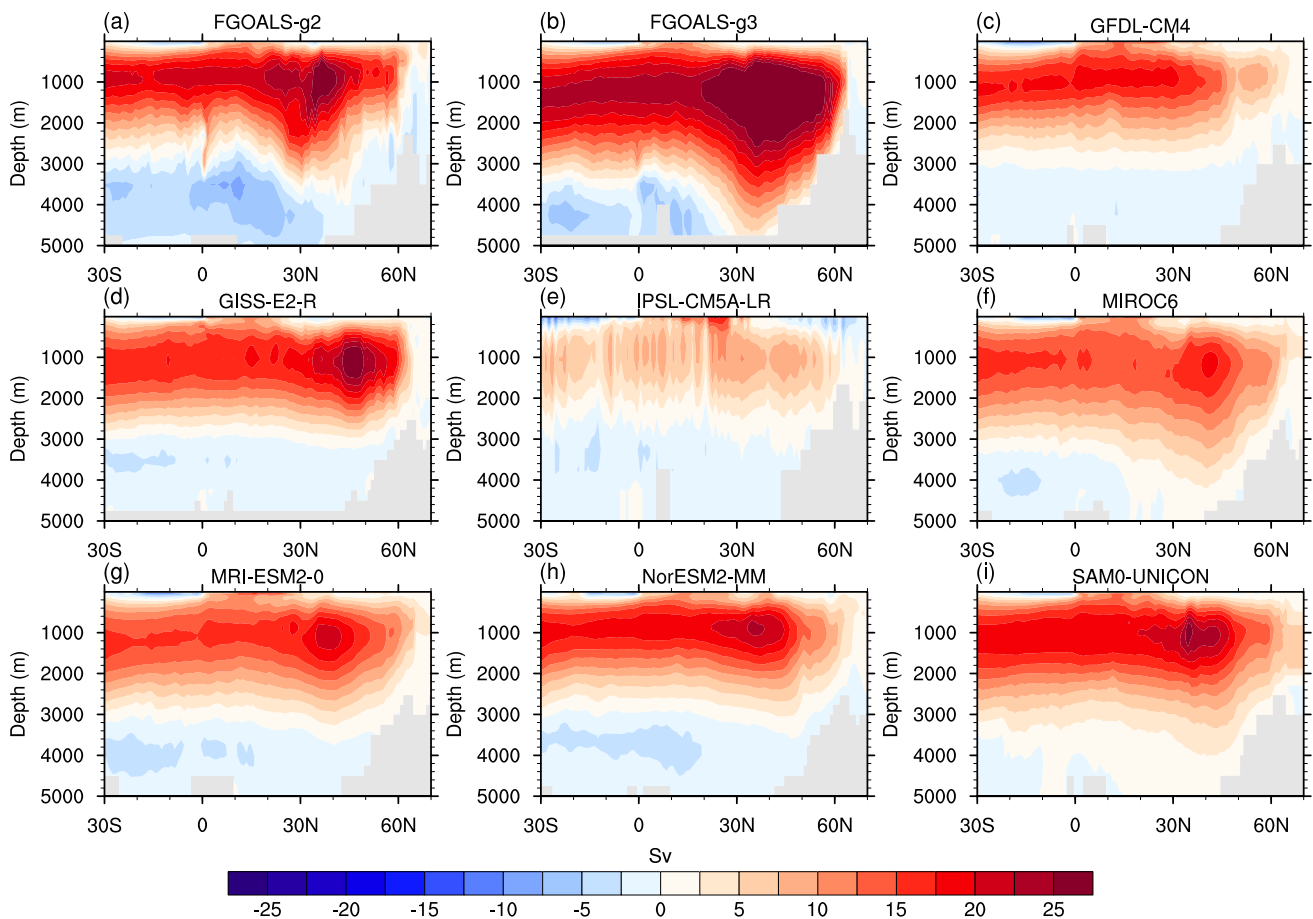


Fig. 1 The mean meridional streamfunction in the Atlantic in the 500-year preindustrial simulations of the 9 models. Names of each model are indicated on the top of each plot. The AMOC strength at

26°N in each model is respectively 23.5 ± 0.9 , 28.5 ± 1.8 , 18.3 ± 1.1 , 18.0 ± 1.1 , 11.5 ± 0.9 , 14.2 ± 1.0 , 17.3 ± 1.0 , 20.7 ± 0.9 , 20.5 ± 1.0 Sv. Annual mean data are used here

the NorESM2-MM, and that the westward signals are relatively weaker in the GFDL-CM4 than in others. The longitudinal discontinuities in signal propagations as shown in the Hovmöller diagram are possibly caused by the bottom topography. For example, the westward propagations are dominant to the west of 20°W – 30°W , the longitude range of the Mid-Atlantic Ridge in the subpolar North Atlantic, however, the eastward propagations are observed mostly to the east of the Mid-Atlantic Ridge. This indicates that the bottom topography may generate or scatter oceanic waves over the subpolar North Atlantic (Chelton and Schlax 1996; Owen et al. 2005; Vianna and Menezes, 2013).

3.3 Potential mechanisms for the dominant timescale of AMOC multidecadal variability

3.3.1 The role of the oceanic baroclinic Rossby wave

The potential mechanisms for the various AMOC dominant timescales in different models might be linked to the

various speeds of the simulated baroclinic Rossby waves in the ocean, which is possibly the physical essence underlying the visible signals of westward temperature propagations. The freely propagating Rossby wave speed could be computed from an eigenvalue problem in the linearized quasi-geostrophic potential vorticity (QGPV) equation (Chelton and Schlax 1996). For the simple case without consideration of mean zonal flow (i.e., $U=0$), the linearized QGPV equation in the continuously stratified ocean is

$$\frac{\partial}{\partial t} \left[\frac{\partial^2}{\partial x^2} + \frac{\partial^2}{\partial y^2} + \frac{\partial}{\partial z} \left(\frac{f_0^2}{N^2(z)} \frac{\partial}{\partial z} \right) \right] \psi + \beta \frac{\partial \psi}{\partial x} = 0 \quad (2)$$

where f_0 , N^2 , β , and ψ respectively denote the Coriolis parameter, the buoyancy frequency (or Brunt-Väisälä frequency), the planetary vorticity gradient ($\beta = df/dy$), and geostrophic streamfunction. The buoyancy frequency in the ocean is

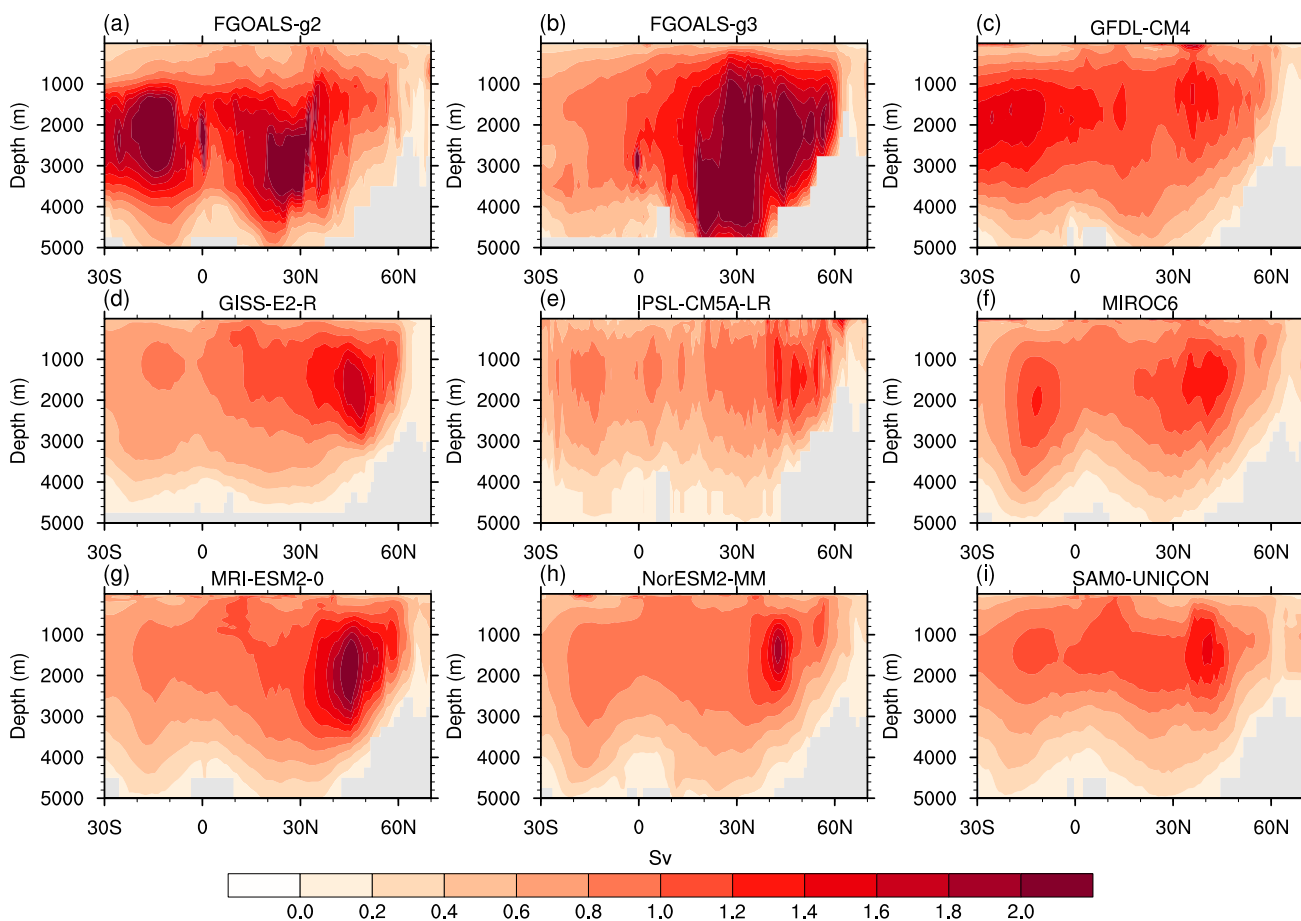


Fig. 2 The standard deviation of the annual mean meridional streamfunction in the Atlantic in the 500-year preindustrial simulations of the 9 models. Names of each model are indicated on the top of each plot

$$N^2(z) = -\frac{g}{\rho_0} \frac{\partial \rho}{\partial z} \tag{3}$$

where g , ρ_0 , and ρ respectively denote the gravitational acceleration, the referenced ocean density, and ocean potential density. Set $\psi = \phi(z)\Psi(x, y)e^{-i\omega t}$, the vertical component of Eq. (2) can be derived as

$$\frac{d}{dz} \left[\frac{f_0^2}{N^2(z)} \frac{d\phi}{dz} \right] - \lambda \phi = 0, \lambda = \frac{\beta k}{\omega} \tag{4}$$

with ϕ , λ , k , and ω denoting eigenfunction, eigenvalue, zonal wavenumber, and circular frequency. The eigenvalue problem is then formed by this vertical structure together with the rigid vertical boundary conditions (vertical velocities vanish at the ocean surface and bottom). The numerical solutions for the eigenvalue and eigenfunction can be obtained based on given N^2 and f_0 (Chelton et al. 1998). In the longwave approximation, the speed magnitude of the first baroclinic Rossby wave is

$$c = \frac{\omega}{k} = \frac{\beta}{\lambda} \tag{5}$$

and the timescale for the wave propagating across the basin is

$$T = \frac{L}{c} \tag{6}$$

where L denotes the basin width. Here, β is set to the value at 52.5°N, the center latitude of 45°N–60°N, and L is set to 3700 km as the mean width between 45°N–60°N in the Atlantic basin. In our calculation, the baroclinic Rossby wave speed over 45°N–60°N in the Atlantic is not sensitive to the choice of β value, such as β at 52.5°N, or the averaged β at 45°N, 52.5°N, and 60°N, etc. Consistently, Huck et al. (1999) found that the mean states and variability patterns related to the meridional overturning circulation have slight differences in the idealized ocean model experiments with β varying realistically and with β -plane centered at 40°N.

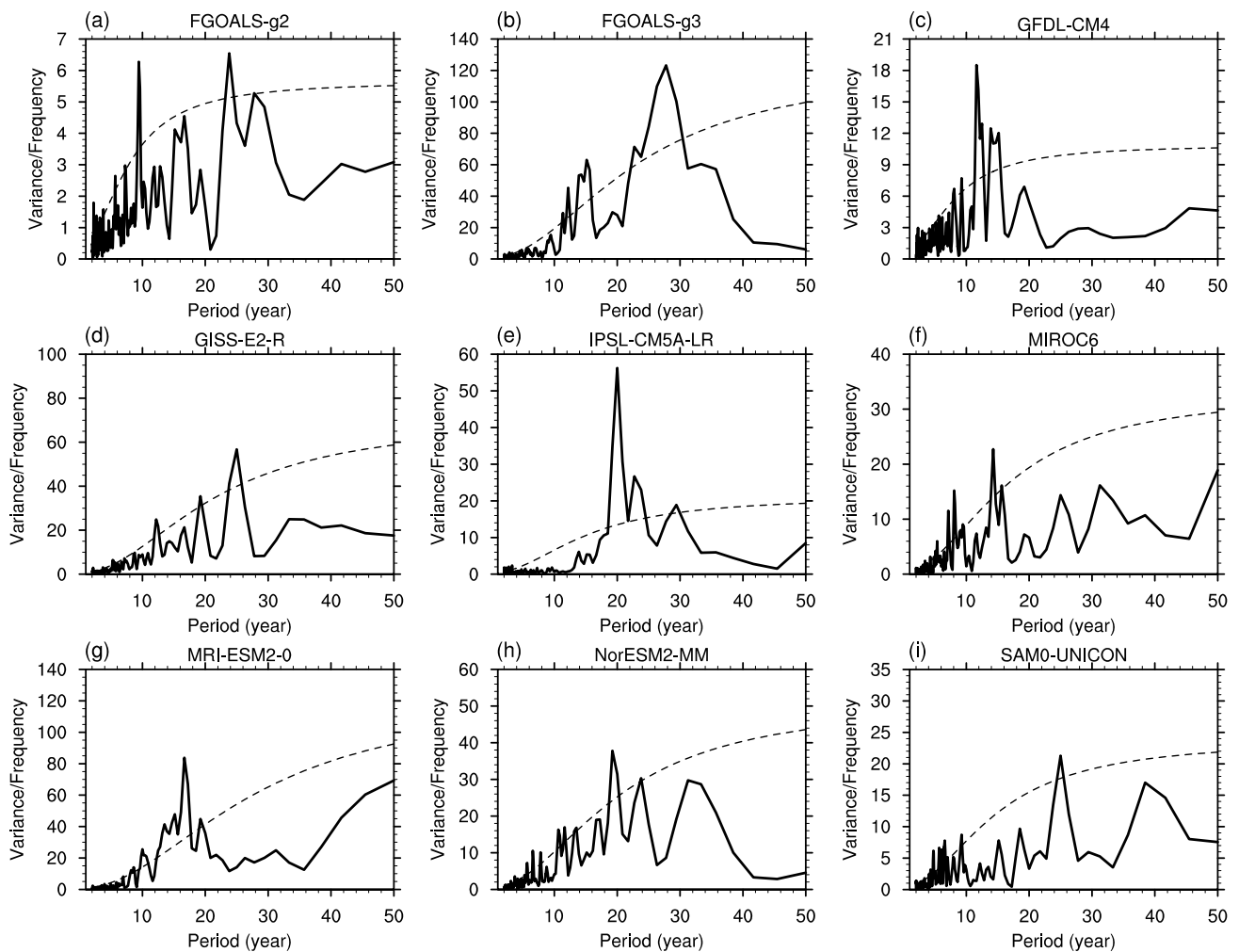
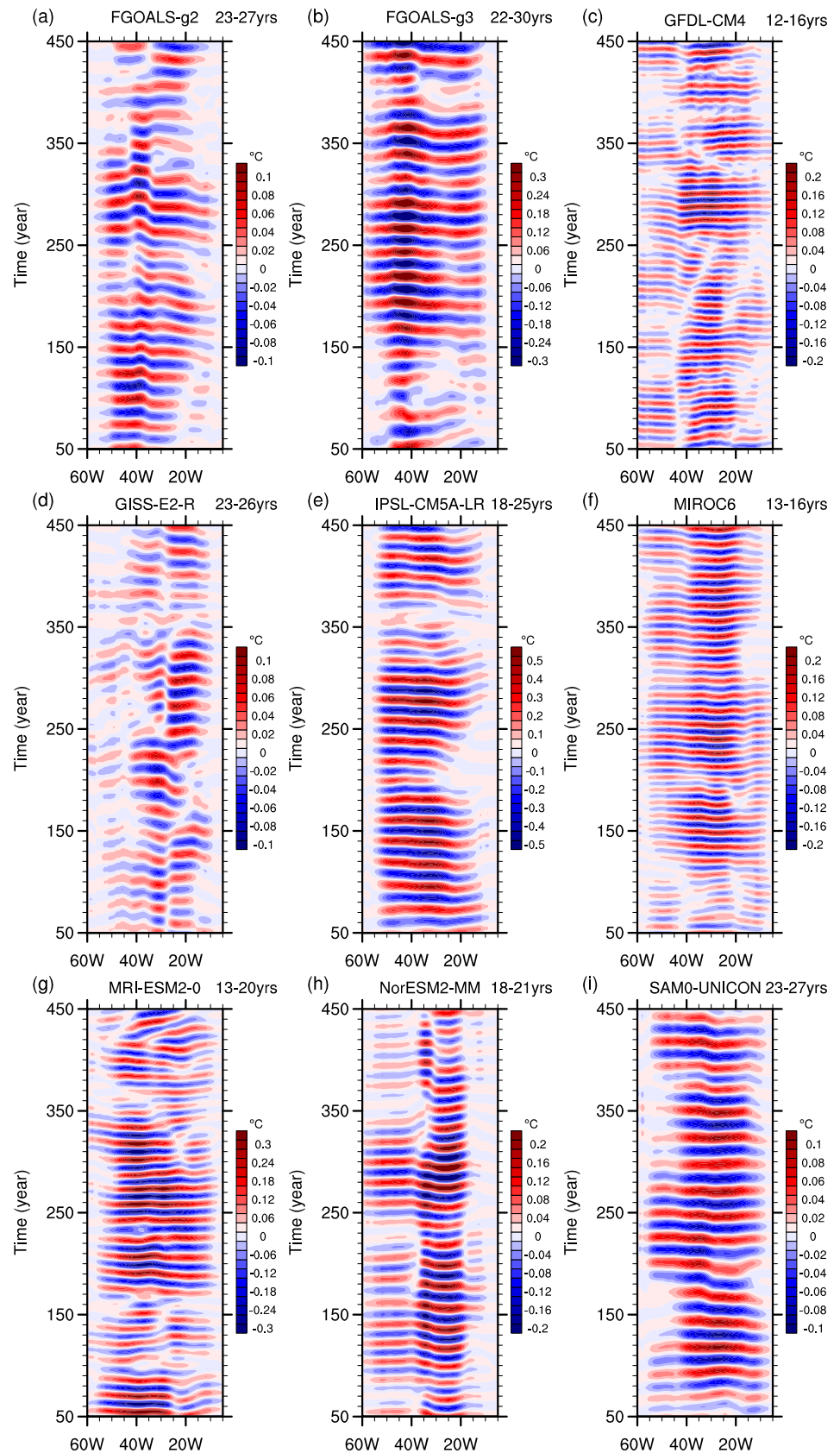


Fig. 3 The power spectrum for the AMOC indices at 45°N in the 500-year preindustrial simulations for the 9 CMIP6/CMIP5 models (solid lines). Names of each model are indicated on the top of each plot. Dashed lines denote the 95% confidence level of the red noise spectrum

As a metric of oceanic vertical stability represented by the buoyancy frequency, ocean stratification is an important modulator for the speed of baroclinic Rossby wave and, in turn, the timescale of AMOC variability (Yang et al. 2012; Wu and Liu 2020). The vertical profiles of buoyancy frequency averaged over the subpolar North Atlantic (45°N–60°N, 0–80°W) in the 9 models are shown together with those in the 3 sets of observations (Fig. 6). In observations (Fig. 6b), buoyancy frequency in the top ~60 m depth from Argo is much smaller than that from the other two, which is possibly due to the short time coverage of Argo such that this mean result may be subject to decadal variability. Most models can capture the realistic vertical structure of the ocean that shown in the mean results of observations (Fig. 6a). An intensely stratified thermocline locates between a mixed layer with weak stratification and a deep layer with relatively uniform properties. Note the largest variation of ocean stratification occurs in the top ~1100 m depth.

We then calculate the speed and basin-crossing timescale of baroclinic Rossby waves over the subpolar North Atlantic (Fig. 7) based on ocean stratifications in models and observations. The baroclinic Rossby wave speeds computed from models are generally consistent with that from observations, in which modeled Rossby waves show a little faster speed than the observed wave (0.0013 m s^{-1}), except IPSL-CM5A-LR simulating a bit slower speed than observations (Fig. 5a, asterisks). Further, the timescales of baroclinic Rossby waves crossing the subpolar North Atlantic basin in most models (~43–78 years) are smaller than the observed timescale (~88 years), except IPSL-CM5A-LR (~99 years) (Fig. 5b, asterisks). However, the AMOC major timescales obtained from the spectral peaks in these models are in the magnitude of about 12–28 years (Fig. 5b, circles). If we compare the baroclinic Rossby wave timescale with the AMOC timescale, we find in each model that the former is much larger (about 3 times) than the latter, which means the

Fig. 4 Hovmöller diagrams of temperature anomalies in the 500-year preindustrial simulations in the 9 models. Names of each model are indicated on top of each plot. In each model, a band-pass filter around the AMOC spectral peak is applied to temperature anomalies, which is averaged over 45°N–60°N, 0–1100 m depth. The time bands used for band-pass filtering are indicated on the top-right of each plot. On each end of the Y-axis, 50 years are omitted because of the filtering. Notice the magnitude of temperature anomalies for each model is different. Time goes upward



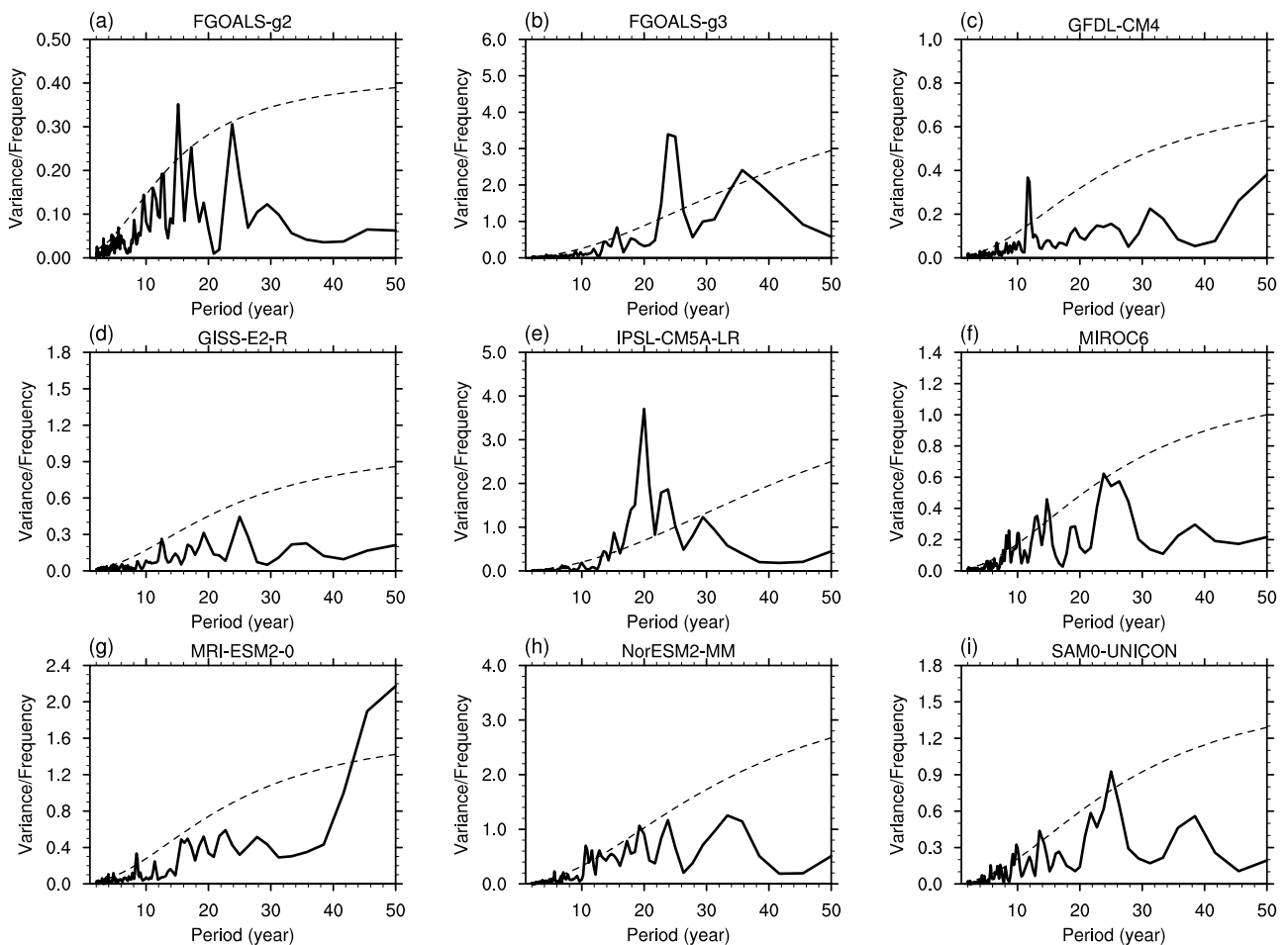


Fig. 5 The power spectrum for the temperature anomalies averaged over 50°N–60°N, 80°W–0°, 0–1100 m depth in the 500-year preindustrial simulations in the 9 models (solid lines). Dashed lines denote the 95% confidence level of the red noise spectrum

baroclinic Rossby wave is too slow to interpret the AMOC variability. Thus, considering the baroclinic Rossby wave propagating on a static background mean flow ($U=0$) does not capture the dominant timescale of AMOC variability. To find a way to improve the estimate of the major timescale of AMOC variability, other factors affecting AMOC variations need to be included.

3.3.2 The role of the mean flow

Considering the mean flow effects may help enhance the estimate of AMOC major timescales, based on the dual roles of the mean zonal flow—the eastward mean advection and the additional westward propagation—in the AMOC variability and the related westward temperature propagating (Sévellec and Fedorov 2013, 2015; Ortega et al. 2015; Muir and Fedorov 2017). Here, we apply the propagating mode formulated in an idealized two-layer ocean model (Sévellec and Fedorov 2013, 2015) to the continuously stratified oceans, in order to generally estimate the contribution of the mean flow effects

to wave propagations and hence AMOC timescales in the 9 models. Particularly, the resulting propagation speed with the consideration of the mean flow effects as well as the baroclinic Rossby wave can be written in the form of

$$c = U - U' - \frac{\beta}{\lambda} \quad (7)$$

where U and U' are the speed magnitude of the mean zonal advection and the additional westward propagation. The negative sign denotes the westward speed direction. Here, $U' = \frac{gh(H-h)}{2Hf_0} \frac{1}{\rho_0} \frac{\partial \bar{\rho}}{\partial y}$ denoted by ocean density is based on the form expressed by ocean temperature and salinity in Sévellec and Fedorov (2013), where $\bar{\rho}$, H , and h is the mean ocean potential density, ocean total depth, and upper ocean thickness, respectively. The ocean potential density including both thermal and saline impacts is used in the calculation of the additional westward propagation. The magnitude of the additional westward propagation (U') is mainly determined by the background meridional density gradient, which is

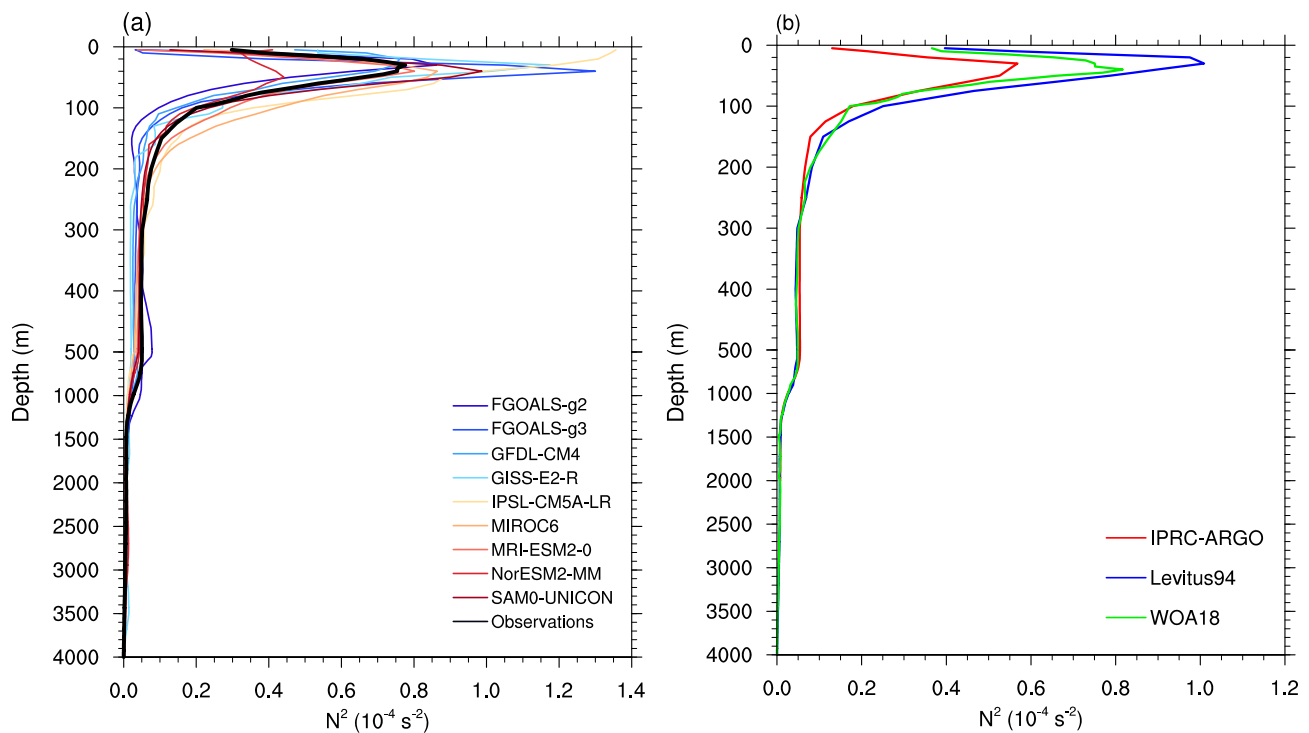


Fig. 6 The mean vertical profiles of the buoyancy frequency (N^2) over the subpolar North Atlantic (45°N – 60°N , 80°W – 0°) in (a) models and (b) observations. Colored lines in (a) denote model results. Thick black line in (a) denotes the average of the 3 observation data-

sets. Colored lines in (b) denote the results of individual observation datasets. Notice two different scales above and below 500 m depth are used

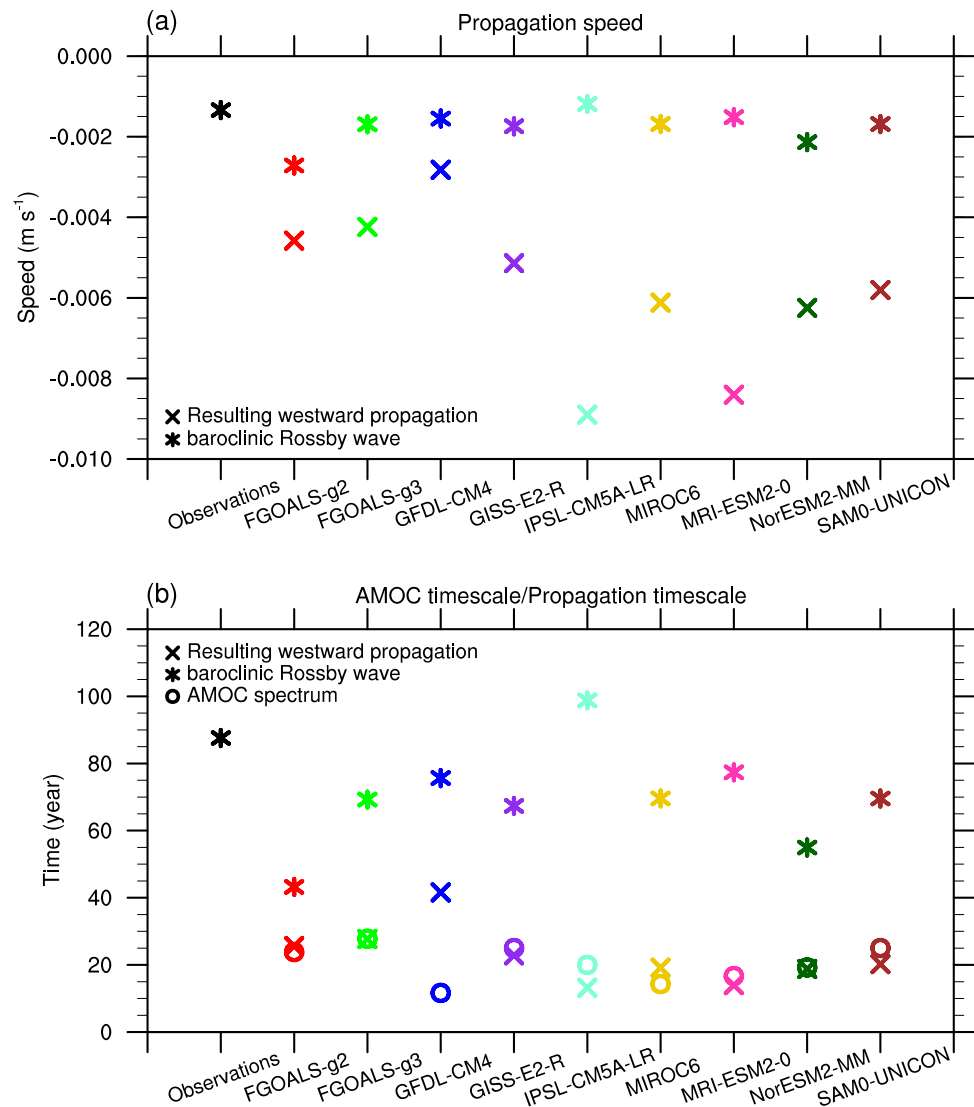
called as thermal Rossby wave (e.g., Te Raa and Dijkstra 2002; Dijkstra et al. 2006). Assume the mean zonal advection (U) is eastward, the background northward density gradient causes a northward potential vorticity gradient, enhances the generalized beta, and therefore induces an additional westward propagation (or thermal Rossby wave). Here, we set $H = 4500$ m in our analyses according to the AMOC vertical structure as well as the Atlantic topography among the models we used (Fig. 1). We set $h = 1100$ m since that the AMOC maximum exists around 1100 m depth in most models (Fig. 1) and that ocean stratification has large changes in the top 1100 m depth (Fig. 6). Since the poor availability in the gridded product of ocean current observations, we only examine the mean flow effects in model simulations.

We consider the mean flow effects in the upper ocean since the deeper layer has little changes. In each model, the vertically averaged (0–1100 m) U and U' show similar spatial patterns with generally inverse signs and different magnitudes, in which large anomalies appear over the Gulf Stream region and to the south of Greenland (Figs. 8, 9). We average U and U' over the subpolar North Atlantic (45°N – 60°N , 80°W – 0° , 0–1100 m) and compute the resulting propagation speed based on Eq. (7). In all models, the resulting propagation speeds with the consideration of the

mean flow effects are westward and faster (Fig. 7a, crosses) than the previous calculations without the mean flow effects (Fig. 7a, asterisks). The increased amount of propagation speeds due to the mean flow effects is distinct from model to model (69%–454%). Further, the basin-crossing timescales of the resulting westward propagation mode with the consideration of the mean flow effects show a nice coincidence with the AMOC timescales almost in all models (Fig. 7b, crosses and circles). Note that in the GFDL-CM4, the resulting westward propagation time (~ 42 years) does not capture the AMOC timescale (~ 12 years) very well. This could be combined with the relatively weak temperature westward propagation in this model (Fig. 4c) and may be related to the dominant eastward currents extending to the coastal England in this model (Fig. 8c). In general, considering the mean flow effects as well as the baroclinic Rossby wave tends to provide a greatly improved estimate of the AMOC major timescales in multiple models. Here we just evaluate the mean flow effects on the wave propagation in a qualitative manner by using Eq. (7), which is not a strictly solved formula aiming to get an accurate computation.

The contributions of the three sources to the resulting propagation speed based on Eq. (7) over the subpolar North Atlantic in the 9 models are shown in Fig. 10. The additional westward propagation serves as the main factor

Fig. 7 Wave characteristics and AMOC timescales in models and observations. **a** the baroclinic Rossby wave speeds (asterisk) and the resulting westward propagation speeds (cross) with the consideration of mean flow effects over the subpolar North Atlantic (45°N–60°N, 80°W–0°). **b** The baroclinic Rossby wave timescales (asterisk), the resulting westward propagation timescales (cross) with the consideration of mean flow effects over the subpolar North Atlantic (45°N–60°N, 80°W–0°), and the dominant AMOC timescales in the 9 models (circle) derived from the respective AMOC spectral peaks. Colored dots denote model results. Black dots denote the average from the 3 observation sets



determining the resulting westward propagation speed and hence the AMOC major timescale. In most models, the mean flow effects as a whole account for a majority of the resulting westward speed, the baroclinic Rossby wave on the other hand takes a relatively small share.

The changes in the mean flow might also play a part in the longitudinal discontinuities in the AMOC-related westward temperature propagations (Fig. 4). We calculate the resulting propagation speeds based on Eq. (7) but with U and U' averaged over the west (80°W–30°W) and the east (20°W–0°) of the Mid-Atlantic Ridge (30°W–20°W). The propagation directions over the two subsections of the North Atlantic are mostly agreeable with the results in Fig. 4: westward propagations to the west of the Mid-Atlantic Ridge and eastward propagations to the east of the Mid-Atlantic Ridge, excepting the uniform westward propagations in FGOALS-g2 and MIROC6.

4 Conclusion and discussion

In this study, we make multi-model analyses of the dominant timescales and underlying mechanisms in the AMOC multidecadal variability using the preindustrial simulations of 9 CMIP6/CMIP5 models. We find dominant AMOC timescales ranging from 12 to 28 years and the relevant evidence of westward spread of temperature anomalies over the subpolar North Atlantic. We attribute these phenomena in the AMOC multidecadal variability partly to the large-scale baroclinic Rossby wave in the ocean, which is largely affected by the state of ocean stratification. However, the calculations based on the baroclinic Rossby wave timescales generally overestimate the AMOC timescales by 182%–650% in these models. Further, we find that the mean flow effects in the subpolar North Atlantic play greater roles in setting the AMOC major timescale, in which the additional westward propagation (i.e.,

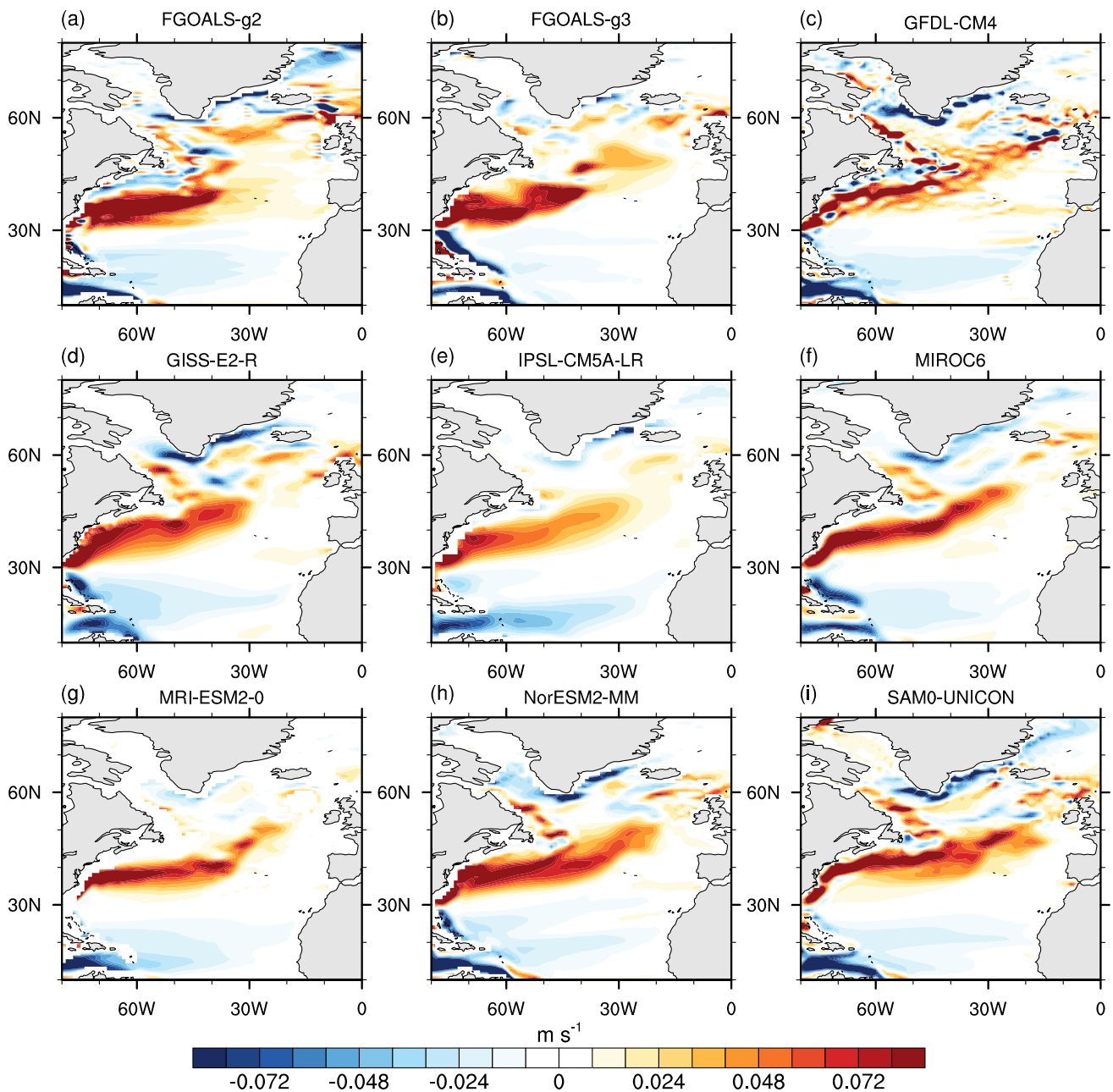


Fig. 8 The mean zonal advection U averaged in 0–1100 m depth over the 500-year simulations in the 9 models

thermal Rossby wave) due to the enhanced mean meridional potential vorticity gradient plays a larger role than the mean eastward advection. The calculations established on the resulting propagation timescales including both the mean flow effects and the baroclinic Rossby wave greatly improve the estimate of AMOC timescales in these models, with the accuracy of 80.83%–357.60% (if excludes GFDL-CM4, 80.83%–134.22%). In summary, the major timescales of AMOC multidecadal variability is generally controlled by the comprehensive effects of the baroclinic Rossby wave and the mean flow effects.

To interpret the AMOC major timescale at 45°N, we discuss the temperature propagation and baroclinic Rossby waves across the subpolar North Atlantic (45°N–60°N) where the majority of models exhibit intense AMOC variations (Fig. 2). This serves as a uniform way to conduct analyses in multiple models. However, the strongest AMOC variability indeed occurs at different latitudes in multiple models (Fig. 2), which indicates that the exact latitude of the temperature propagation and Rossby wave responsible for AMOC variability is possibly different among models (Ortega et al. 2015; Cheng et al. 2016; Muir and Fedorov

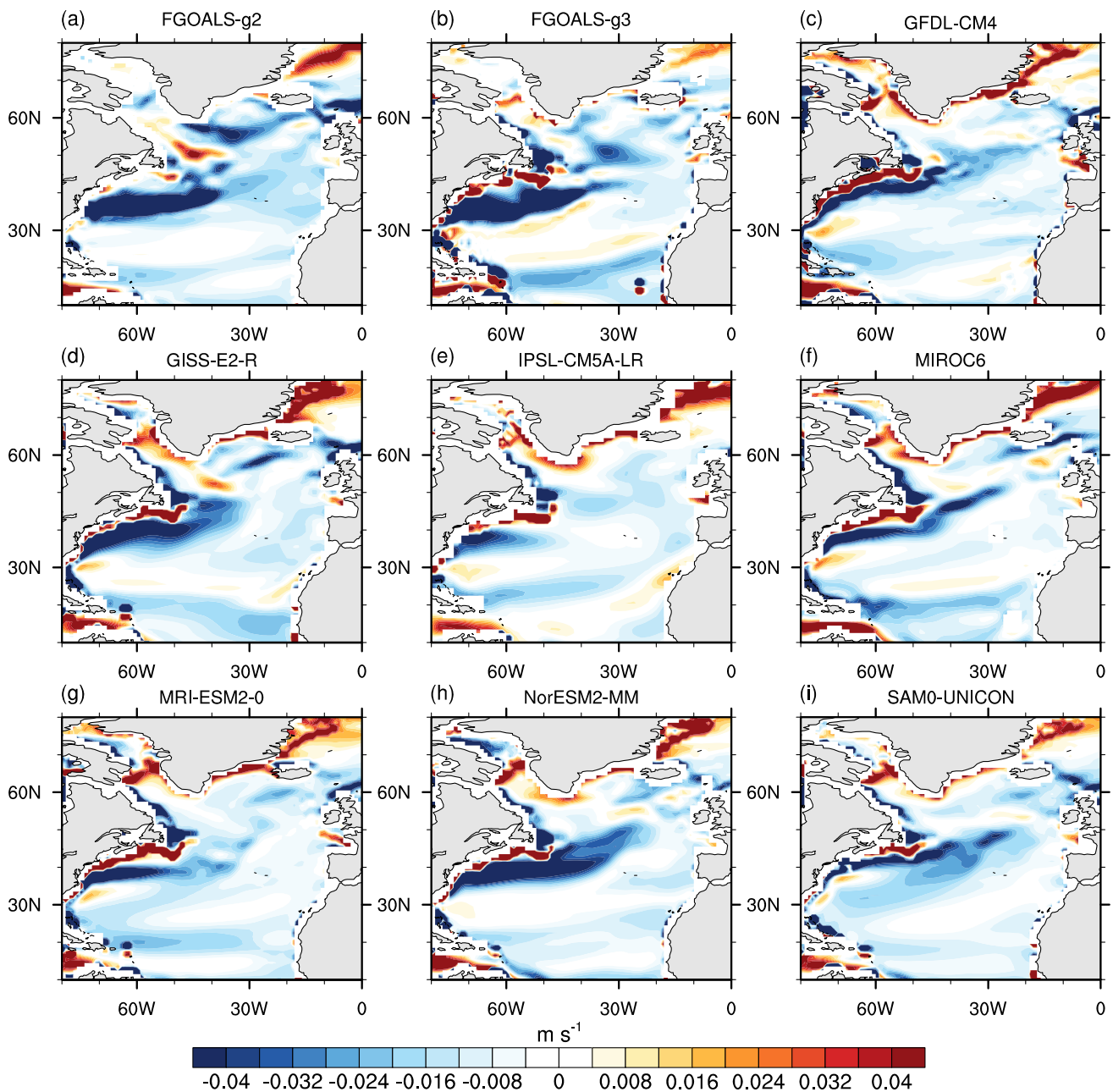


Fig. 9 The additional westward propagation U' averaged in 0–1100 m depth over the 500-year simulations in the 9 models

2017). Previous studies have investigated the dependence on the latitude of the baroclinic Rossby wave speed and suggested that in high-latitude oceans the baroclinic Rossby wave propagates on decadal timescales while in low-latitude oceans it propagates on interannual timescales (Chelton and Schlax 1996). The much slower Rossby waves in high-latitude oceans are possibly due to the larger planetary vorticity, the weaker stratification (Yang et al. 2012; Sévellec and Fedorov 2013), or the smaller Rossby deformation scale (Tulloch et al. 2009).

The calculation of the mean flow effects here regards the upper ocean thickness as a simple constant of 1100 m in all models, neither different constants for individual model nor a variable as a function of spatial positions. This might be another caveat of our study. The sensitivity of the AMOC timescale to the upper ocean thickness in an idealized model has been illustrated in Sévellec and Fedorov (2013) that increasing the upper ocean thickness causes a faster westward wave speed and a shorter timescale, which is also true in the 9 models used in our study.

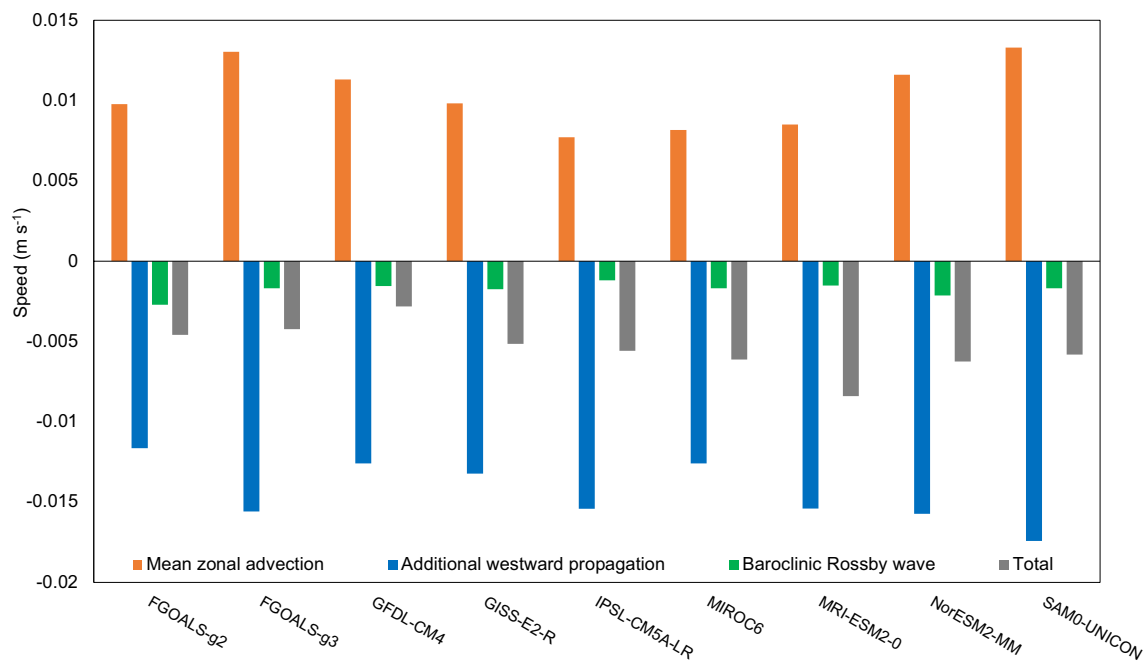


Fig. 10 Contributions of the three sources (the mean zonal advection, the additional westward propagation, and the baroclinic Rossby wave) to the resulting propagation speed based on Eq. (7) in the 9

models. The results are calculated over the subpolar North Atlantic (45°N–60°N, 80°W–0°)

The Rossby wave mode in an idealized two-layer model has many simplifications such that the inclusion of the mean flow effects may not always produce westward propagation speed (Sévellec and Fedorov 2013, 2015). At least in the 9 models we examined, the mean flow effects generate a westward speed tendency ($|U'| > |U|$) over the subpolar North Atlantic and make the resulting basin-crossing time closer to the AMOC timescale. The relative magnitude of U and U' is however model dependent, which might rely on the temperature and salinity patterns in the ocean, ocean–atmosphere interactions, etc. Other models well simulating the multidecadal AMOC variability may have $|U'| < |U|$, such as the CESM2-FV2 and the CESM2-WACCM, in which an eastward speed tendency could be produced by the mean flow effects.

Our study mainly explores the AMOC-related temperature anomalies spreading across the subpolar North Atlantic basin. Besides temperature anomalies, some model studies have displayed the propagating features in salinity or density anomalies associated with the AMOC variability, which also has clear westward spreading signals over the subpolar North Atlantic (Tulloch and Marshall 2012; Ortega et al. 2015; Sévellec and Fedorov 2013, 2015). The vertical structures of density or temperature anomalies over the subpolar North Atlantic have large uncertainties among the models used in this study and do not match well with the vertical structure of the first baroclinic Rossby wave. The mechanisms for the formation of the oceanic vertical structure related to the AMOC multidecadal

variability when the mean flow effects are considered need further investigations.

Acknowledgements This work was supported by the National Natural Science Foundation of China (42141019, 41831175, 91937302, and 41721004) and the Second Tibetan Plateau Scientific Expedition and Research Program (2019QZKK0102). Xichen Li is supported by the National Natural Science Foundation of China (Grant No. 41976193 and 42176243).

Data availability The CMIP6/CMIP5 data are freely available at <https://esgf-node.llnl.gov/search/cmip6/> and <https://esgf-node.llnl.gov/search/cmip5/>. The IPRC Argo plus Aviso altimetry data can be download from <https://argo.ucsd.edu/data/argo-data-products/>. The Levitus94 world-ocean atlas is available at <https://iridl.ldeo.columbia.edu/SOURCES/LEVITUS94/index.html>. The WOA18 world-ocean atlas is available at <https://www.nodc.noaa.gov/OC5/woa18/>. Partial data of this study could be downloaded on this website: <https://drive.google.com/drive/folders/1d9D16g0n7BiQpjjHndJBpPQCTRfZULMQ?usp=sharing>.

Declarations

Conflict of interest The authors have no competing interests to declare that are relevant to the content of this article.

References

Argo (2020) Argo float data and metadata from Global Data Assembly Centre (Argo GDAC). SEANOE

- Armstrong E, Valdes P, House J, Singarayer J (2017) Investigating the Impact of CO₂ on Low-Frequency Variability of the AMOC in HadCM3. *J Clim* 30(19):7863–7883
- Årthun M, Wills RC, Johnson HL, Chafik L, Langehaug HR (2021) Mechanisms of decadal North Atlantic climate variability and implications for the recent cold anomaly. *J Clim* 34(9):3421–3439
- Buckley MW, Marshall J (2016) Observations, inferences, and mechanisms of the Atlantic Meridional overturning circulation: a review. *Rev Geophys* 54(1):5–63
- Buckley MW, Ferreira D, Campin J-M, Marshall J, Tulloch R (2012) On the relationship between decadal buoyancy anomalies and variability of the Atlantic meridional overturning circulation. *J Clim* 25(23):8009–8030
- Chelton DB, DeSzoek RA, Schlax MG, El Naggar K, Siwertz N (1998) Geographical variability of the first baroclinic Rossby radius of deformation. *J Phys Oceanogr* 28(3):433–460
- Chelton DB, Schlax MG (1996) Global observations of oceanic Rossby waves. *Science* 272(5259):234–238
- Cheng J, Liu Z, Zhang S, Liu W, Dong L, Liu P, Li H (2016) Reduced interdecadal variability of Atlantic meridional overturning circulation under global warming. *Proc Natl Acad Sci* 113(12):3175–3178
- Chylek P, Folland C, Frankcombe L, Dijkstra H, Lesins G, Dubey M (2012) Greenland ice core evidence for spatial and temporal variability of the Atlantic Multidecadal Oscillation. *Geophys Res Lett* 39(9).
- Colin de Verdière A, Huck T (1999) Baroclinic instability: an oceanic wavemaker for interdecadal variability. *J Phys Oceanogr* 29(5):893–910
- Cunningham SA, Kanzow T, Rayner D, Baringer MO, Johns WE, Marotzke J et al (2007) Temporal variability of the Atlantic meridional overturning circulation at 26.5 N. *Science* 317(5840):935–938
- Dijkstra HA, Te Raa L, Schmeits M, Gerrits J (2006) On the physics of the Atlantic multidecadal oscillation. *Ocean Dyn* 56(1):36–50
- Feng QY, Dijkstra H (2014) Are North Atlantic multidecadal SST anomalies westward propagating? *Geophys Res Lett* 41:541–546. <https://doi.org/10.1002/2013GL058687>
- Frankcombe L, Dijkstra H (2009) Coherent multidecadal variability in North Atlantic sea level. *Geophys Res Lett* 36(15)
- Frankcombe L, Dijkstra H, Von der Heydt A (2008) Sub-surface signatures of the Atlantic Multidecadal Oscillation. *Geophys Res Lett* 35(19).
- Frankcombe LM, Von Der Heydt A, Dijkstra HA (2010) North Atlantic multidecadal climate variability: an investigation of dominant time scales and processes. *J Clim* 23(13):3626–3638
- Gastineau G, Mignot J, Arzel O, Huck T (2018) North Atlantic ocean internal decadal variability: role of the mean state and ocean-atmosphere coupling. *J Geophys Res Oceans* 123(8):5949–5970
- Griffies SM, Bryan K (1997) Predictability of North Atlantic multidecadal climate variability. *Science* 275(5297):181–184
- Huck T, Verdière AC, de, Weaver A. J. (1999) Interdecadal variability of the thermohaline circulation in box-ocean models forced by fixed surface fluxes. *J Phys Oceanogr* 29:865–892
- Johnson HL, Marshall DP (2002) A theory for the surface Atlantic response to thermohaline variability. *J Phys Oceanogr* 32(4):1121–1132
- Kawase M (1987) Establishment of deep ocean circulation driven by deep-water production. *J Phys Oceanogr* 17(12):2294–2317
- Killworth PD, Chelton DB, de Szoek RA (1997) The speed of observed and theoretical long extratropical planetary waves. *J Phys Oceanogr* 27(9):1946–1966
- Knight JR, Folland CK, Scaife AA (2006) Climate impacts of the Atlantic multidecadal oscillation. *Geophys Res Lett* 33(17)
- Levitus S, Boyer TP (1994) World ocean atlas 1994. volume 4. temperature. National Environmental Satellite, Data, and Information Service, Washington
- Levitus S, Burgett R, Boyer TP (1994) World Ocean Atlas 1994. Vol. 3, Salinity
- Liu Z (1999) Planetary wave modes in the thermocline: Non-Doppler-shift mode, advective mode and Green mode. *Q J R Meteorol Soc* 125(556):1315–1339
- Liu Z (2012) Dynamics of interdecadal climate variability: a historical perspective. *J Clim* 25(6):1963–1995
- Locarnini M, Mishonov A, Baranova O, Boyer T, Zweng M, Garcia H et al (2018) World ocean atlas 2018, volume 1: Temperature
- Ma X, Liu W, Allen RJ, Huang G, Li X (2020) Dependence of regional ocean heat uptake on anthropogenic warming scenarios. *Science Advances* 6(45):eabc0303
- Ma X, Liu W, Burls NJ, Chen C, Cheng J, Huang G, Li X (2021) Evolving AMOC multidecadal variability under different CO₂ forcings. *Clim Dyn* 1–18
- MacMartin DG, Zanna L, Tziperman E (2016) Suppression of Atlantic meridional overturning circulation variability at increased CO₂. *J Clim* 29(11):4155–4164
- McCarthy G, Frajka-Williams E, Johns WE, Baringer MO, Meinen CS, Bryden H et al (2012) Observed interannual variability of the Atlantic meridional overturning circulation at 26.5 N. *Geophys Res Lett* 39(19).
- Moat BI, Smeed DA, Frajka-Williams E et al (2020) Pending recovery in the strength of the meridional overturning circulation at 26 N. *Ocean Sci* 16:863–874
- Muir LC, Fedorov AV (2017) Evidence of the AMOC interdecadal mode related to westward propagation of temperature anomalies in CMIP5 models. *Clim Dyn* 48(5–6):1517–1535
- Ortega P, Mignot J, Swingedouw D, Sévellec F, Guilyardi E (2015) Reconciling two alternative mechanisms behind bi-decadal variability in the North Atlantic. *Prog Oceanogr* 137:237–249
- Owen GW, Willmott AJ, Abrahams ID, Mansley H (2005) The scattering of Rossby waves from finite abrupt topography. *Geophys Astrophys Fluid Dyn* 99(3):219–239
- Rossby C-G (1939) Relation between variations in the intensity of the zonal circulation of the atmosphere and the displacements of the semi-permanent centers of action. *J Mar Res*
- Sévellec F, Fedorov AV (2013) The leading, interdecadal eigenmode of the Atlantic meridional overturning circulation in a realistic ocean model. *J Clim* 26(7):2160–2183
- Sévellec F, Fedorov AV (2015) Optimal excitation of AMOC decadal variability: links to the subpolar ocean. *Progr Oceanogr* 132:287–304
- Sicre M-A, Yiou P, Eiríksson J, Ezat U, Guimbert E, Dahhaoui I et al (2008) A 4500-year reconstruction of sea surface temperature variability at decadal time-scales off North Iceland. *Quatern Sci Rev* 27(21–22):2041–2047
- Sutton RT, Hodson DL (2005) Atlantic Ocean forcing of North American and European summer climate. *Science* 309(5731):115–118
- Taylor KE, Stouffer RJ, Meehl GA (2012) An overview of CMIP5 and the experiment design. *Bull Am Meteor Soc* 93(4):485–498
- Te Raa LA, Dijkstra HA (2002) Instability of the thermohaline ocean circulation on interdecadal timescales. *J Phys Oceanogr* 32(1):138–160
- Tulloch R, Marshall J, Smith KS (2009) Interpretation of the propagation of surface altimetric observations in terms of planetary waves and geostrophic turbulence. *J Geophys Res* 114:C02005
- Vianna ML, Menezes VV (2013) Bidecadal sea level modes in the North and South Atlantic Oceans. *Geophys Res Lett* 40(22):5926–5931

- Wu S, Liu Z-Y (2020) Decadal variability in the North Pacific and North Atlantic under global warming: the weakening response and its mechanism. *J Clim* 33(21):9181–9193
- Yang Y, Wu L, Fang C (2012) Will global warming suppress North Atlantic tripole decadal variability? *J Clim* 25(6):2040–2055
- Zhang J, Zhang R (2015) On the evolution of Atlantic meridional overturning circulation fingerprint and implications for decadal predictability in the North Atlantic. *Geophys Res Lett* 42(13):5419–5426
- Zhang L, Wang C (2013) Multidecadal North Atlantic sea surface temperature and Atlantic meridional overturning circulation variability in CMIP5 historical simulations. *J Geophys Res Oceans* 118(10):5772–5791
- Zhang R, Delworth TL (2006) Impact of Atlantic multidecadal oscillations on India/Sahel rainfall and Atlantic hurricanes. *Geophys Res Lett* 33(17)
- Zhang R, Sutton R, Danabasoglu G, Kwon Y, Marsh R, Yeager SG et al (2019) A review of the role of the Atlantic meridional overturning circulation in Atlantic multidecadal variability and associated climate impacts. *Rev Geophys* 57(2):316–375
- Zweng M, Seidov D, Boyer T, Locarnini M, Garcia H, Mishonov A et al (2019) *World ocean atlas 2018, volume 2: Salinity*

Publisher's Note Springer Nature remains neutral with regard to jurisdictional claims in published maps and institutional affiliations.

Springer Nature or its licensor holds exclusive rights to this article under a publishing agreement with the author(s) or other rightsholder(s); author self-archiving of the accepted manuscript version of this article is solely governed by the terms of such publishing agreement and applicable law.